

# PROCEEDINGS OF SPIE

[SPIDigitalLibrary.org/conference-proceedings-of-spie](https://SPIDigitalLibrary.org/conference-proceedings-of-spie)

## C-RED 2 ER: an extended range SWIR camera for hyperspectral imaging

De Kernier, Isaure, Wanwanscappel, Yann, Boutolleau, David, Carmignani, Thomas, Clop, Fabien, et al.

Isaure De Kernier, Yann Wanwanscappel, David Boutolleau, Thomas Carmignani, Fabien Clop, Philippe Feautrier, J. L. Gach, Stephane Lemarchand, Eric Stadler, "C-RED 2 ER: an extended range SWIR camera for hyperspectral imaging," Proc. SPIE 11997, Optical Components and Materials XIX, 119970V (4 March 2022); doi: 10.1117/12.2624018

**SPIE.**

Event: SPIE OPTO, 2022, San Francisco, California, United States

# C-RED 2 ER : an extended range SWIR camera with applications in hyperspectral imaging

Isaure de Kernier<sup>a,\*</sup>, Yann Wanwanscappel<sup>a</sup>, David Boutolleau<sup>a</sup>, Thomas Carmignani<sup>a</sup>, Fabien Clop<sup>a</sup>, Philippe Feautrier<sup>a</sup>, J.L. Gach<sup>a</sup>, Stephane Lemarchand<sup>a</sup>, Eric Stadler<sup>a</sup>

<sup>a</sup> First light Imaging S.A.S., Europarc Ste Victoire Bât 5, Route de Valbrillant, 13590 Meyreuil, France

\* isaure.dekernier@first-light.fr; phone +33 442612920 ; www.first-light-imaging.com

## ABSTRACT

The development of extended range detectors based on InGaAs technology is a recent breakthrough in imaging. Taking advantage of the technological bricks developed for the C-RED 2 camera, First Light Imaging has integrated extended range InGaAs sensors and explored the possibilities offered by this technology. The C-RED 2 ER camera can support two detectors with shifted sensitivity. The cameras and their performances are described in detail in this paper.

The C-RED 2 ER camera can operate with different readout modes and achieve high-speed frame processing to optimize the output image. The camera is capable of running at 600 full frames per second with image corrections applied. This is particularly relevant, as the lattice mismatch artefacts of the extended InGaAs technology can be a major drawback for its use in imaging and sensing applications.

It is expected that the shifted spectral sensitivity of the C-RED 2 ER cameras will enable the development of systems dedicated to hyperspectral imaging, for waste sorting in particular. A proof of concept device based on a First Light Imaging camera was developed to demonstrate the performances of high-speed SWIR cameras when integrated in a push-broom type device. The result of this experiment is briefly reported in this paper.

**Keywords:** Fast infrared camera, extended range InGaAs, hyperspectral, sorting, eSWIR, imaging

## 1. INTRODUCTION

### 1.1 The C-RED 2 Extended Range camera

Lattice-match InGaAs has an optical cut-off wavelength at 1.7  $\mu\text{m}$ . This detector technology is mature and integrated in several commercial cameras – such as the C-RED 2 from First Light Imaging [1, p. 2], [2, p. 2]. Progress in band-gap engineering has enabled the development of new detectors. The detection cut-off wavelength can be increased by tuning the indium composition of the  $\text{In}_x\text{Ga}_{1-x}\text{As}$  compound [3]. C-RED 2 ER is – to our knowledge - the first commercial camera integrating a VGA format InGaAs detector with shifted spectral bandwidth .

The C-RED 2 extended range camera was developed as a versatile platform to integrate extended range InGaAs VGA detectors. Currently, two versions of the camera are available : the C-RED 2 ER 1.9  $\mu\text{m}$ , integrating an extended range detector sensitive up to 1.9  $\mu\text{m}$  and the C-RED 2 ER 2.2  $\mu\text{m}$  integrating a detector sensitive up to 2.2  $\mu\text{m}$ .

The development of this camera answers a specific need of the hyperspectral imaging community, as the 1.7  $\mu\text{m}$  cut-off wavelength limits the use cases, in particular regarding the plastic waste sorting [4].



Figure 1. The C-RED 2 ER camera commercialized by First Light Imaging.

### 1.2 Extended range sensors

The camera can integrate either of two planar InGaAs detectors with shifted sensibility ranges :

- 1.1  $\mu\text{m}$  to 1.9  $\mu\text{m}$
- 1.2  $\mu\text{m}$  to 2.2  $\mu\text{m}$

Both are VGA (640 x 512 pixels) detectors with a 15  $\mu\text{m}$  pixel pitch and with peak quantum efficiency > 70%. The two detectors have a two-stage thermoelectric cooler integrated, which enables a cooling capability up to 60°C.

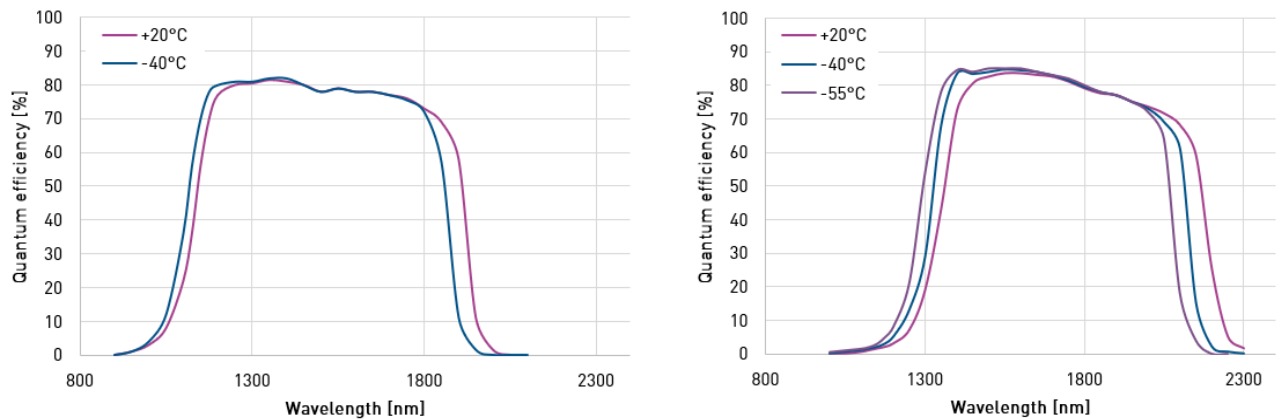


Figure 2. Quantum efficiency of the two sensors which can be integrated in C-RED 2 ER

### 1.3 Main camera characteristics

The main characteristics of the C-RED 2 ER camera are the following :

- Extended range InGaAs 640 x 512 sensor
- Global shutter - snapshot
- Up to 600 FPS in full frame, 32 000 FPS in cropping mode
- Peak quantum efficiency > 70%
- Supported readout modes : correlated double sampling (CDS), nondestructive readout (IMRO), ITR/IWR

- Embedded double-stage TEC cooler, air (fan) cooling down to  $-15^{\circ}\text{C}$  and water cooling down to  $-55^{\circ}\text{C}$
- CameraLink® full and USB 3.0 interfaces
- Factory calibrated correction maps for lattice mismatch artefacts

#### 1.4 Extended range SWIR detector technologies

The main purpose of the extended range cameras is to detect wavelengths beyond  $1.7\ \mu\text{m}$  which is the limit of standard InGaAs. Other sensor technologies are available to achieve this aim, and significant progress has been made in new detector architectures [3]. The easy integrability and operation of the extended InGaAs technology makes it particularly attractive for industrial applications.

Cameras based on HgCdTe (MCT) sensors offer a sensitivity range spanning from  $0.8\ \mu\text{m}$  to  $2.5\ \mu\text{m}$ . However, the mass production of MCT is complex : poor material uniformity, low yield, high cost, *etc.* This strongly limits the industrial potential of the technology. Additionally, the deep cooling requires the use of cryogenics, making the camera unfit for many industrial application.

Type-II superlattice (T2SL) detector technology is based on a repeating sequence of nanometric layers of different semiconductor materials. This enables to tune the cut-off wavelength from SWIR to LWIR by modifying the thickness and composition of the individual layers. Although low dark current can be theoretically expected from the technology, the cameras based on T2SL still require a very deep cooling (typically down to 200 K).

Extended range InGaAs is made of bulk material (alloy of different compounds), in our case In-rich InGaAs grown on InP substrate. Band-gap engineering of the compound semi-conductor enables to tune the cut-off wavelength. This technology benefits from the maturity of standard InGaAs based detectors.

Quantum dot photodiode arrays is another available technology for extended SWIR imaging. The band-gap of the QD material can be tuned, however, the quantum efficiency of these detectors is still very low, although this may be improved in the future.

Note that having a camera which is sensitive to wavelength beyond those that are relevant for the specific use case can be counterproductive as the useful signal will be polluted by the temperature-induced dark signal. This is a direct consequence of the spectral distribution of thermal radiance emitted by the environment surrounding the camera as illustrated in Figure 3. The dark current signal reduces the useful dynamic range of the sensor.

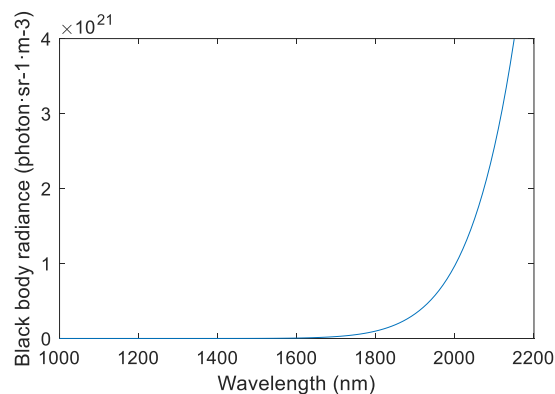


Figure 3. Spectral density function of thermal black body radiance at  $25^{\circ}\text{C}$  as a function of wavelength.

## 2. MEASURED C-RED 2 ER PERFORMANCES

The characterizations are made on housed cameras with scientific grade sensors, operating at their nominal recommended operation temperature ( $-40^{\circ}\text{C}$  for C-RED 2 ER 1.9  $\mu\text{m}$  and  $-55^{\circ}\text{C}$  for C-RED 2 ER 2.2  $\mu\text{m}$ ). The raw data processing is done on all the pixels, including those affected by lattice-mismatch artefacts.

### 2.1 Quantum efficiency

Quantum efficiency provides the conversion rate of incident photons into photo-induced electrons in the sensor, as a function of wavelength. It is a key feature of the camera as it describes the sensibility of the sensor to signal of specific wavelength and flux level. Quantum efficiency can be evaluated on the full camera system using a calibrated monochromator bench.

Figure 4 illustrates the shift of the low cut-off wavelength that can be observed on a C-RED 2 ER 2.2  $\mu\text{m}$  camera. We have observed that the operating temperature has limited effect on the peak sensitivity value.

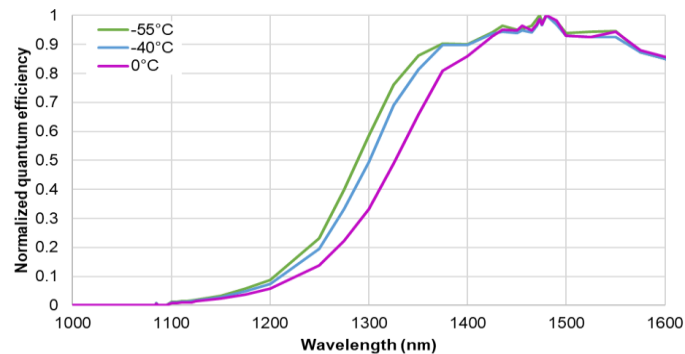


Figure 4. Measured low cut-off wavelength shift as a function of temperature for C-RED 2 ER 2.2  $\mu\text{m}$  (normalized)

### 2.2 System conversion gain

The system gain is measured using the Photon Transfer Curve method : the camera is illuminated with a flat field of varying intensity through an integrating sphere. The temporal variance is plotted against the mean level (see Figure 5). The system gain, expressed in electrons per ADU, is the inverse of the slope, determined with a linear regression. The system gain is a property of the sensor capacitors. The cameras can be operated in three different capacitor modes : High gain, Medium gain and Low gain, offering a relevant range of system gain values. The capacitors are a specification of the ROIC. Typical values : High gain (low full well) capacitor offers system gain of 2.4 e-/ADU, Medium gain offers 8.3 e-/ADU and Low gain (high full well) offers 92 e-/ADU.

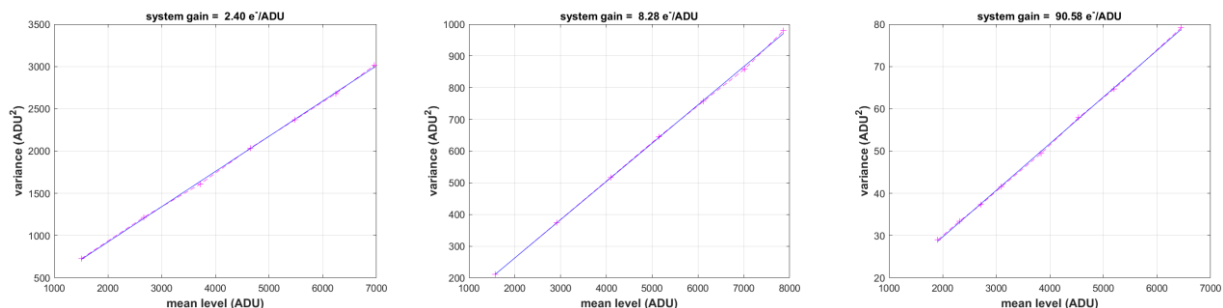


Figure 5. Typical photon transfer curves at the three available gains for a C-RED 2 ER 2.2  $\mu\text{m}$  camera

### 2.3 Readout noise

Readout noise is evaluated in dark conditions with a cooled sensor, at 50  $\mu\text{s}$  integration time. The contribution of the dark current to the total temporal noise is considered negligible at low temperature and very short integration times. Typically, the C-RED 2 ER 1.9  $\mu\text{m}$  achieves a readout noise  $< 50\text{ e-}$  while C-RED 2 ER 2.2  $\mu\text{m}$  readout noise is  $< 40\text{ e-}$ .

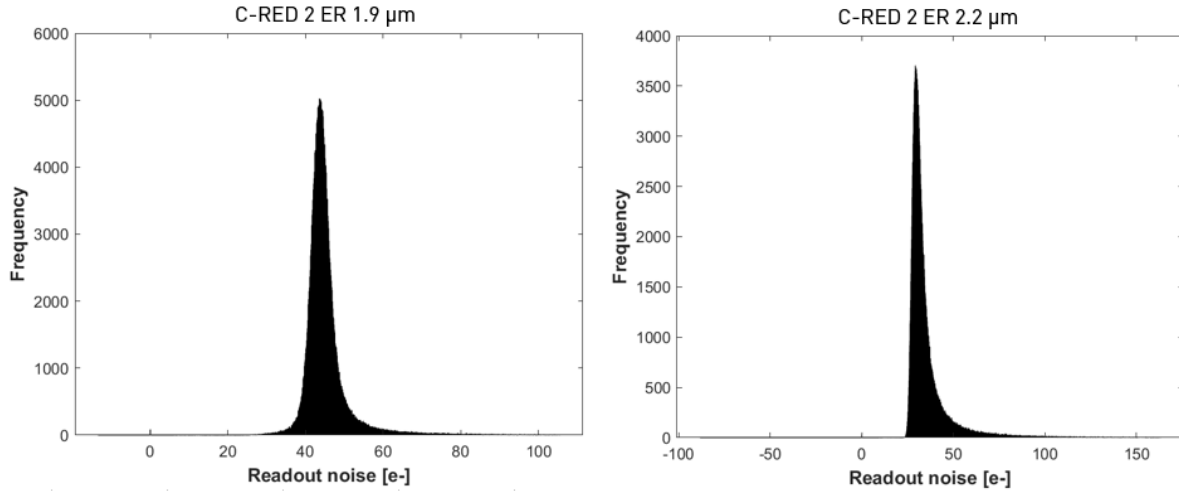


Figure 6. Typical readout noise distributions

### 2.4 Dark current

The dark current is the main concern when using the cameras at long exposure times, as it fills the capacitors with a noisy signal that does not carry any useful information. The quantification of this signal is important to understand the limitations of the camera. However, as illustrated earlier, the fact that extended range cameras are sensitive to the thermal background of the scene makes it difficult to isolate the dark current. Here, dark current is evaluated from the linear regression of the dark signal of the High gain capacitor as a function of integration time, for a cooled camera looking at a 20°C target. For C-RED 2 ER 2.2  $\mu\text{m}$ , dark signal is typically 110 000  $\text{e-}/\text{pixel}/\text{s}$ , while for a C-RED 2 ER 1.9  $\mu\text{m}$  it is typically 11 000  $\text{e-}/\text{pix}/\text{s}$ . The dark current measured values are not entirely consistent for the three capacitors, the reason for this is still unclear.

### 2.5 Linearity

Linearity is evaluated by exposing the camera to a flat field illumination of fixed intensity and varying the integration time. The response nonlinearity is the deviation from the linear regression in the range of 10 to 90 % of the full well. For both cameras, the typical non-linearity is  $< 1\%$ . Typical full wells are reported in Table 1.

Table 1. Full well typical values

|                              | High gain | Medium gain | Low gain |
|------------------------------|-----------|-------------|----------|
| C-RED 2 ER 1.9 $\mu\text{m}$ | 34 ke-    | 132 ke-     | 1.53 Me- |
| C-RED 2 ER 2.2 $\mu\text{m}$ | 34 ke-    | 130 ke-     | 1.47 Me- |

### 3. OPERATION

The raw cosmetics of the extended range detectors is strongly degraded by lattice-mismatch artefacts. Operability and non-uniformity can be optimized with proper operation of the sensor, enabled by the C-RED 2 ER cameras.

#### 3.1 Impact of lattice-mismatch artefacts

The compound composition of the extended range sensors, tuned to reach the target bandgap, strongly affects their cosmetics. While standard InGaAs is a lattice-matched compound, the extended InGaAs sensors are affected by crystal lattice-mismatch. The mismatch between InGaAs and InP substrate induces a mechanical strain in the matrix, which can propagate to the active region of the sensor. The induced defects affect sensor cosmetics through dark current and pixel responsivity mainly. Due to a worse mismatch, the C-RED 2 ER 2.2  $\mu\text{m}$  is more deteriorated than the C-RED 2 ER 1.9  $\mu\text{m}$ . Figure 11 compares two images acquired with cooled sensors and 1.66 ms exposure time.

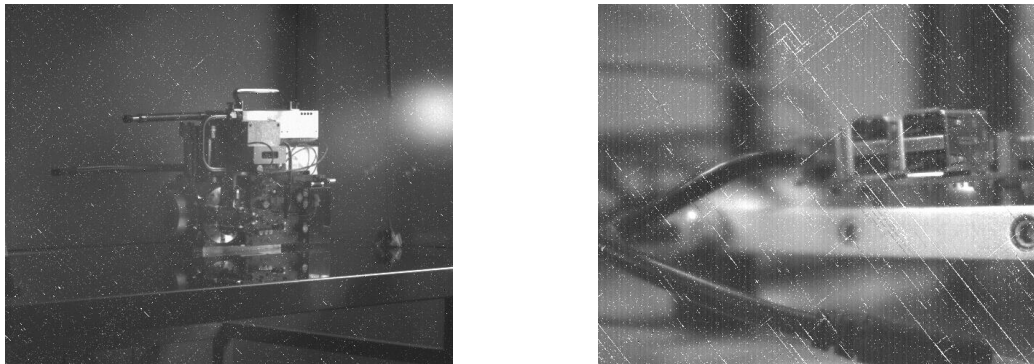


Figure 7. Raw images from the C-RED 2 ER 1.9  $\mu\text{m}$  (left) and C-RED 2 ER 2.2  $\mu\text{m}$  (right)

As a result of the strong dependence of the dark current of individual pixels on the cosmetic defects, there are several evident strategies to mitigate the poor cosmetics. First, use the large capacitor (low gain) rather than the small capacitor (high gain) of the sensor. Second, decrease the sensor operating temperature. And lastly, work at short integration times.

Depending on the use case, one of the three strategies may be more evident than the others to implement, which is why the camera operation does not impose a specific operation mode. All three methods will optimize the pixel operability, *i.e.*, the percentage of pixels with response output deviation within  $\pm 30\%$  of mean value. The effect of temperature and integration time is studied for the C-RED 2 ER 2.2  $\mu\text{m}$  and summarized in Figure 8.

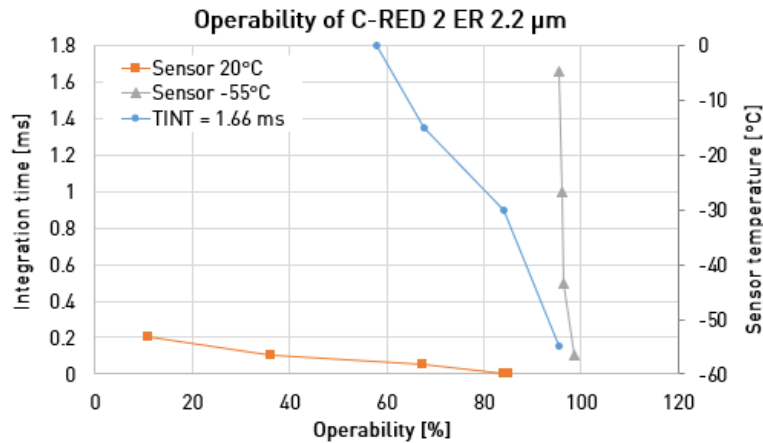


Figure 8. Operability as a function of sensor temperature and integration time (at 20°C) for C-RED 2 ER 2.2  $\mu\text{m}$ .

### 3.2 Non-uniformity maps

The non-uniformity maps of the cameras provide information on the gain and offset of each pixel relative to the average value of the full frame. They give an experimental model for the behavior of individual pixels. Understanding these maps enable to optimize the operation of the camera. The maps in Figure 9 and Figure 10 are representative results from one C-RED 2 ER 1.9 $\mu\text{m}$  and one C-RED 2 ER 2.2 $\mu\text{m}$  operating at 600 FPS, maximum integration time and respectively -40°C and -55°C.

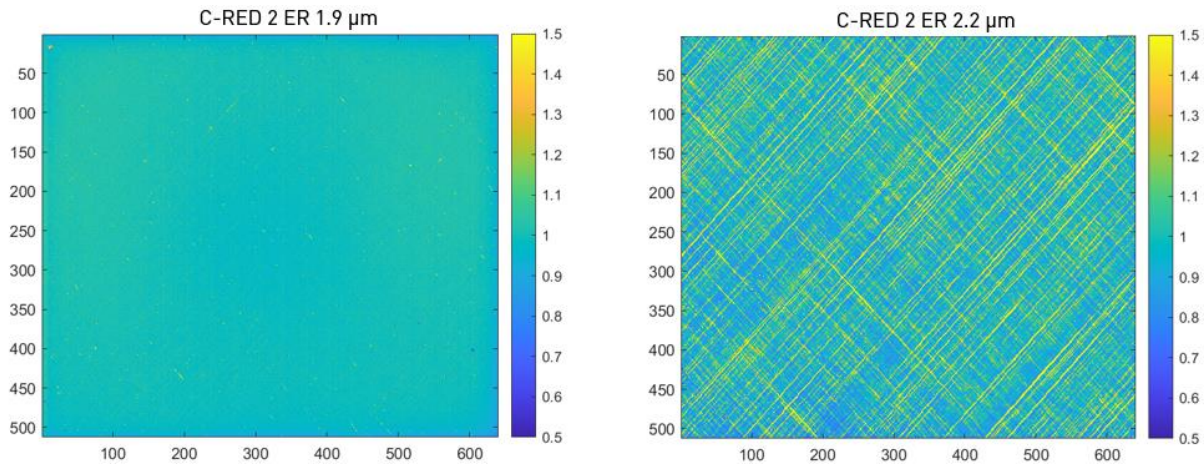


Figure 9. Typical gain maps

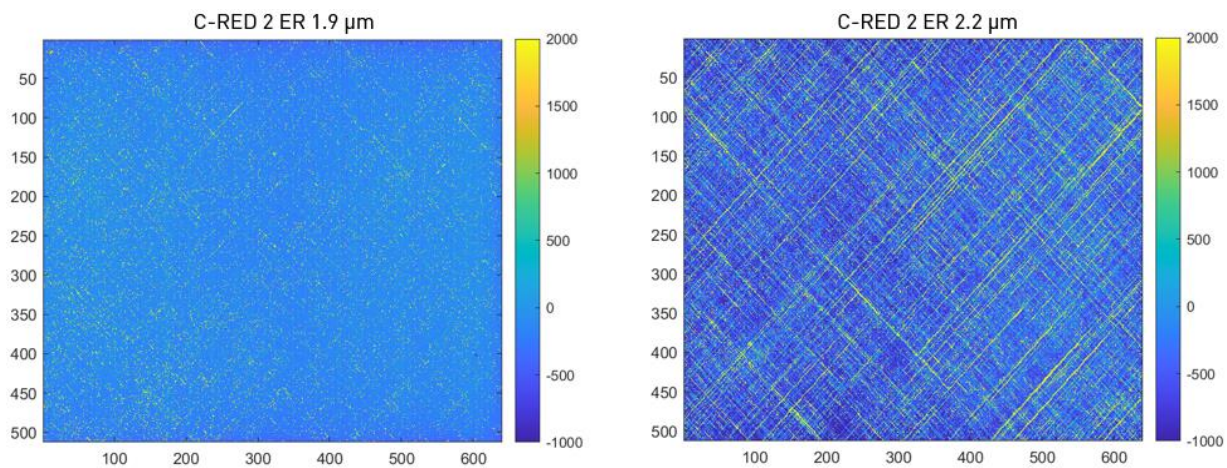


Figure 10. Typical offset maps

These maps are embedded in the camera and can be applied in real time, thanks to a Xilinx embedded FPGA, without any limitation on the camera framerate. They effectively correct for the non-uniformity of the sensor in the dark and the non-uniformity of the sensor's response to illumination, as illustrated in Figure 11. Pixels that have reached saturation cannot be corrected, and this is the main limitation for the applicability of the correction method. These pixels can be detected early on the non-uniformity maps and classified as *bad pixels*, their correction either by the nearest neighbor value or the weighted average of the nearest neighbors can then be applied.

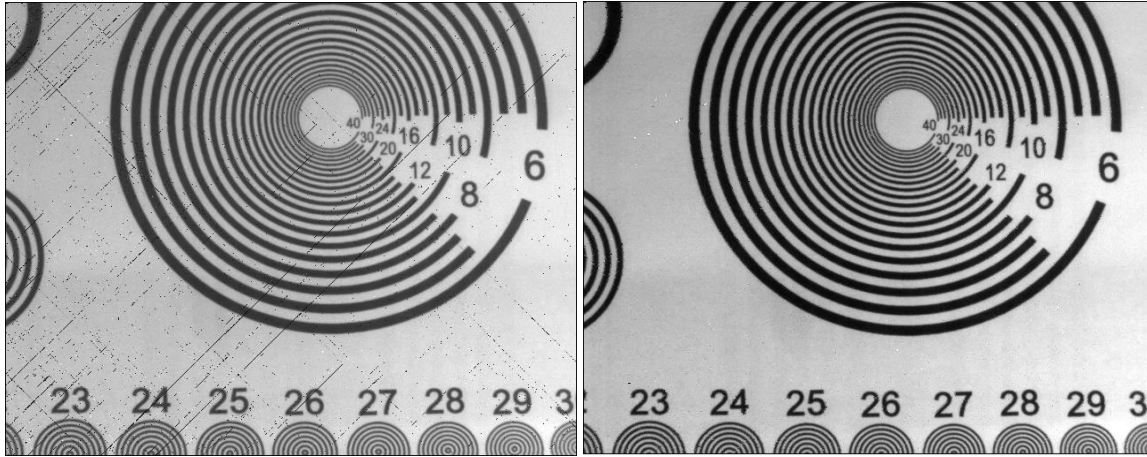


Figure 11. C-RED 2 ER 2.2  $\mu\text{m}$  image after non-uniformity correction, without and with bad pixel correction

### 3.3 Using the camera in a hyperspectral imaging system

By combining a spectral dimension to two spatial dimensions, hyperspectral imaging is a key technology to discriminate and classify materials with high purity rates, especially in the waste sorting industry. However, this technique faces several issues. First, the unique spectral signature which results from the chemical structure of the material and enables its accurate classification, is generally found in a specific and confined region of the wavelength spectrum, and beyond 1.7  $\mu\text{m}$  for some applications, such as plastic discrimination. The second issue faced by industrial waste sorting is that the hyperspectral imaging system limits the speed of the conveyor belt on which the objects are placed. The C-RED 2 ER cameras with sensitivity ranges overcoming the usual limitation of InGaAs, either 1.1 to 1.9  $\mu\text{m}$  or 1.2 to 2.2  $\mu\text{m}$  and running at 600 Hz in full frame will nicely answer the challenges.

A proof-of-concept system was developed with a C-RED 3 camera [5], which has the same throughput characteristics (speed, interface, *etc.*) as C-RED 2 ER. When integrated in a push-broom type hyperspectral imaging system, the C-RED 3 camera offers 230 spectral bands with 3.4 nm resolution on a 35° (horizontal) by 20° (vertical) field of view. A throughput of 1.2 kHz was reached. The high sensitivity of the detector enabled to use the full speed allowed by the camera and still detect signal of low light applications with a high SNR value. When operating in this way, it was possible to retrieve the chemical composition maps of complex objects, such as plastic bottles with caps and stickers.

## 4. CONCLUSION

The C-RED 2 ER camera can integrate one of two extended range InGaAs detectors. The first will offer sensitivity from 1.1 to 1.9  $\mu\text{m}$ , and the other one from 1.2 to 2.2  $\mu\text{m}$ . They both combine low noise, high speed (600 full frames per second) performances with a resolution of 640 x 512 pixels (VGA). With lattice-mismatch artefact compensation maps embedded in the camera, C-RED 2 ER overpasses the usual cosmetic drawback of the extended InGaAs technology. With a double TEC cooling system, the camera is a straightforward solution for imaging in the far end of the SWIR spectrum without the cryogenic cooling required for HgCdTe. Hence, it can be expected that C-RED 2 ER will be a key component in the development of high speed hyperspectral imaging systems.

## REFERENCES

- [1] P. Feautrier *et al.*, “C-RED 2 InGaAs 640x512 600-fps infrared camera for low order wavefront sensing,” in *Adaptive Optics Systems VI*, Austin, United States, Jul. 2018, p. 68. doi: 10.1117/12.2313545.
- [2] R. K. Gibson, R. Oppenheimer, C. T. Matthews, and G. Vasisht, “Characterization of the C-RED 2: a high-frame rate near-infrared camera,” *J. Astron. Telesc. Instrum. Syst.*, vol. 6, no. 01, p. 1, Nov. 2019, doi: 10.1117/1.JATIS.6.1.011002.
- [3] B. Chen, Y. Chen, and Z. Deng, “Recent Advances in High Speed Photodetectors for eSWIR/MWIR/LWIR Applications,” *Photonics*, vol. 8, no. 1, p. 14, Jan. 2021, doi: 10.3390/photronics8010014.
- [4] S. Serranti, L. Fiore, G. Bonifazi, A. Takeshima, and H. Takeuchi, “Microplastics characterization by hyperspectral imaging in the SWIR range,” presented at the SPIE Future Sensing Technologies, Tokyo, Japan, Nov. 2019. doi: 10.1117/12.2542793.
- [5] J.-L. Gach *et al.*, “C-RED 3: A SWIR camera for FSO applications,” in *Free-Space Laser Communications XXXII*, San Francisco, United States, Mar. 2020, p. 14. doi: 10.1117/12.2545823.